

# Exploring the temperature and composition dependence of the ionic transport in solid-state battery composites

Yannik Rudel<sup>a</sup>, Marvin A. Kraft<sup>b</sup> Lukas Ketter<sup>a,c</sup>, Wolfgang G. Zeier<sup>a,b,c,\*</sup>

*<sup>a</sup>Institute of Inorganic and Analytical Chemistry, University of Münster, Corrensstrasse 28/30, 48149 Münster, Germany*

*<sup>b</sup>Institut für Energie- und Klimaforschung (IEK), IEK-12: Helmholtz-Institut Münster, Forschungszentrum Jülich, Corrensstrasse 46, Münster 48149, Germany*

*<sup>c</sup>International Graduate School of Battery Chemistry, Characterization, Analysis, Recycling and Application (BACCARA), University of Münster, 48149 Münster, Germany*

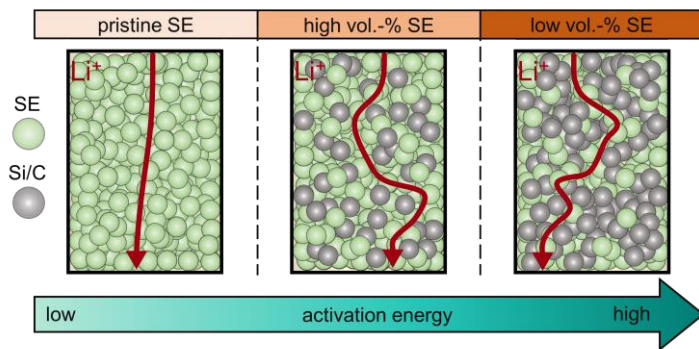
\* [wzeier@uni-muenster.de](mailto:wzeier@uni-muenster.de)

## Keywords

activation energy, effective transport, solid-state batteries, transmission line modelling

## Abstract

Solid-state electrolytes offer a promising avenue in energy storage. In the context of lithium-based batteries not only from an energy density perspective but also by eliminating issues such as freezing of the liquid electrolyte at low temperatures and the performance limitations associated with that. In solid-state batteries the solid electrolytes are not only used in separators, but needed in composite electrodes. However, the transport properties of solid-state battery composites are often investigated at room temperature, while the temperature dependence of effective ion transport as a function of volume fraction remains underexplored. Therefore, this work investigates the effective ionic transport in composites of multiple sulfide-based solid electrolytes with Si/C as the active material, as a function of composition and temperature. Analyzing impedance spectra with a transmission line model, this work reveals changes in activation barrier and with that temperature-dependence of ion-transport upon varying the volume ratios. This finding emphasizes the importance of considering the activation energy in solid-state battery design in order to tailor battery performance to the temperature range of application.



Surprisingly, electrode composites in solid-state batteries show changes in the activation energy of ionic transport and thus differences in their temperature dependence with varying solid electrolyte content. The changing activation barrier with composition is expected to strongly affect the compositional choice depending on the targeted operational range.

## Introduction

Advancements in battery technology are essential for enabling the widespread adoption of electric vehicles as this sector of battery application is set to grow rapidly in the foreseeable future. [1] The temperature limitations associated with traditional liquid electrolytes have become apparent, issues such as freezing of the liquid electrolyte at low temperatures and thus sudden reduction in conductivity have prompted the need for new solutions to improve battery performance. [2] One promising solution to overcome the drawbacks of liquid electrolytes is the implementation of solid-state electrolytes. Unlike their liquid counterparts, solid electrolytes eliminate the risk of sudden drops in conductivity as they are already solid and show an Arrhenius-like behavior over a wider range of temperature. [3] The implications of this holds significant meaning for real-world applications, particularly in the context of enhancing the efficiency and reliability of batteries in diverse environmental conditions. The choice of anode material is another crucial aspect influencing battery performance. As the dense lithium metal anode in solid-state batteries exhibit performance limitations at low temperatures other common active materials like graphite or high capacity alternatives like silicon are being considered as a substitute. [4,5] While some dense silicon anodes have shown promising performance, their areal loading remains limited which is why Si-based solid-state composite anodes are most often explored. Their cycle stability however suffer more dramatically from volume changes upon de-/lithiation. [6–8] This work employs a silicon on graphite (Si/C) composite material with a graphite content of 92 wt.-% – 93 wt.-%, which addresses the volume expansion concerns as carbon not only functions as an active material but also act as a buffer for the volume expansion. [9] This Si/C composite was employed before showing that larger solid electrolyte volume fractions lead to better solid-state battery performance due to faster lithium ion transport in the composite. [10] Additionally, Rana *et al.* investigated the dependence of silicon based composites on the size of active material particles and the ionic conductivity of the chosen electrolyte, indicating that a faster electrolyte and smaller active material particles lead to improved electrochemical performance. [11]

The temperature-dependent performance of solid-state batteries has been explored in the past. For instance, Kato *et al.* showed that thick electrode setups can adequately perform at room temperature, if the tortuosity factor is sufficiently low or lithium ion conductivity of the solid electrolyte is sufficiently high. [12] Some information on the conductivity dependence of low temperature performance where provided by Peng *et al.* [13] by employing  $\text{Li}_{5.5}\text{PS}_{4.5}\text{Cl}_{1.5}$  at room temperature and  $-20\text{ }^{\circ}\text{C}$  at various C-rates and over up to 200 cycles. They show that the fast-conducting solid electrolyte can enable adequate low-temperature performance for solid-

state batteries, however at a limited cathode active material loading of 2.5 mg/cm<sup>2</sup>. More extensive temperature studies of multiple solid-state battery architectures were performed by Lu *et al.* [14] showing that degradation or passivating layers may limit low-temperature performance of solid-state composite cathodes. However, avoiding those cathode limitations results in promising low temperature performance down to even -40 °C, facilitated by low active material loadings (3.8 mg/cm<sup>2</sup>) and a highly conductive solid electrolyte (~10 mS·cm<sup>-1</sup>). For these temperature-dependent investigations the composition of the composites was also pushed towards high solid electrolyte and carbon additive contents, linked to the effective transport in solid-state electrodes, a recently more widely discussed topic. Dewald *et al.* [15] and Minnmann *et al.* [16] were able to show that balancing volume fractions and by this the electronic and ionic conductivity in cathode composites is crucial for optimal performance. Hendriks *et al.* showed this to be also true for LiMnO<sub>2</sub>/Li<sub>3</sub>InCl<sub>6</sub> composites. [17] Zhang *et al.* gave insight in the composition dependence in LiCoO<sub>2</sub> based composites by showing that capacity and cyclability of these composites is majorly influenced by their composition. [18] Additionally, Naik *et al.* investigated cathode performance in relation the active material content giving insights into the relation of electrode thickness and current density dependence of solid-state electrodes. They were able to show that a carbon binder as a secondary phase might not be beneficial for cell performance by giving preferred regimes of active material and carbon content in relation to electrode capacity. [19] Furthermore, Zahnow *et al.* investigated the impact of porosity in NCM cathode material on the electronic and ionic conductivity, showing a non-trivial behavior of the effective conductivities and corresponding activation energies. [20]

With the temperature- and composition- dependence of ion transport in electrode composites investigated, their interdependence, i.e. parallel examination of both remains underexplored. Therefore, in this work, ionic conductivities of electrode composites are investigated as a function of Si/C to solid electrolyte (SE = Li<sub>6</sub>PS<sub>5</sub>Cl, Li<sub>5.5</sub>PS<sub>4.5</sub>Cl<sub>1.5</sub>, and Li<sub>6</sub>PS<sub>5</sub>Br) volume ratio and temperature by impedance analyses with a transmission line model (TLM). This work shows, that changes in volume fractions ( $\phi$ ) of the active material leads to changes in the activation energy for ionic transport in composites. The faster increase of impedances at lower temperatures for high volume fractions of active material, shows that the focus in solid electrolyte research should not only be to find high ionic conductivities at room temperature, but also as low activation barriers as possible to achieve stable solid-state battery performance across a wide range of temperatures. It further shows that for low-temperature operation lower active material loadings may be necessary if much faster solid electrolytes cannot be developed.

## Experimental Section

### Electrolyte Preparation and characterization

All materials and samples were handled in argon atmosphere ( $p(\text{O}_2) \leq 0.1$  ppm,  $p(\text{H}_2\text{O}) \leq 3$  ppm). The solid electrolytes  $\text{Li}_6\text{PS}_5\text{Cl}$ ,  $\text{Li}_{5.5}\text{PS}_{4.5}\text{Cl}_{1.5}$ , and  $\text{Li}_6\text{PS}_5\text{Br}$  were prepared in 3 g batches using the precursors  $\text{Li}_2\text{S}$  (Alfa-Aesar, 99.9%),  $\text{LiCl}$  (Alfa-Aesar, 99%),  $\text{LiBr}$  (Alfa-Aesar, 99.99%),  $\text{P}_2\text{S}_5$  (Sigma-Aldrich 99%) in stoichiometric ratios, mixed in an agate mortar and homogenized by manual grinding for 15 min. Afterwards the powder was hand pressed into pellets ( $d = 10$  mm) and transferred into pre-dried (dynamic vacuum at 800 °C for 2 h) and carbon-coated quartz glass ampoules. The ampoules were sealed under vacuum and annealed in a tube furnace at 550 °C for 14 days in case of the  $\text{Li}_6\text{PS}_5\text{Cl}$  and  $\text{Li}_6\text{PS}_5\text{Br}$ .  $\text{Li}_{5.5}\text{PS}_{4.5}\text{Cl}_{1.5}$  was annealed at 450 °C for 3 days twice, with intermediate regrinding and subsequent pelletizing as described. All products were hand-ground in an agate mortar for further use and characterization. The purity of the solid electrolytes was confirmed by X-ray powder diffraction of the samples sealed in borosilicate glass capillaries spinning during data collection (Stoe STADI P,  $2\theta = 10^\circ - 80^\circ$ ,  $\lambda(\text{Cu K}\alpha_1) = 1.54$  Å, with a Dectris mythen1K detector) (Figure S1). [21]

### Composite preparation

Composites of the synthesized solid electrolytes and Si/C-particles were prepared with different nominal volumetric ratios targeting 30 vol.-%, 40 vol.-% and 50 vol.-% solid electrolyte content. The equivalent weight ratios were calculated using the respective densities (Table SI). The mixing was performed in 200 mg batches for 15 min using a mini shaker mill (Fritsch, PULVERISETTE 23) in a 15 mL  $\text{ZrO}_2$  cup using 15  $\text{ZrO}_2$  balls ( $\varnothing = 3$  mm) at 45 Hz. The Si/C composite material is described elsewhere. [22]

### Cell assembly and Electrochemical measurements

All cells were assembled in a custom-made PEEK cylinder with an inner diameter of 10 mm surrounded by a brass casing. Stainless-steel stamps were employed for pressing and current collectors. [18] Before any measurements were conducted, the cells were held under pressure (50 MPa) for five hours to ensure equilibrated pressure in the cell. [23] Cells for potentiostatic impedance spectroscopy of pristine solid electrolytes were prepared with 200 mg of only the respective argyrodite-type solid electrolyte. Cells for the determination of effective ionic transport properties in the composites using the TLM were prepared by first adding 80 mg of

$\text{Li}_6\text{PS}_5\text{Cl}$  as a separator into the cell and pre-pressing using a manual screw-press, followed by adding 20 mg of the respective composite to each side of the separator.

Potentiostatic electrochemical impedance measurements of the pristine argyrodites as well as the symmetric cells for transmission line modelling were performed at temperatures between  $-40\text{ }^{\circ}\text{C}$  and  $60\text{ }^{\circ}\text{C}$  using a BioLogic SP-300 Potentiostat (7 MHz - 50 mHz, 15 points per decade, excitation voltage = 10 mV). The temperature was increased in  $10\text{ }^{\circ}\text{C}$  increments, with additional room-temperature steps prior and after the temperature ramp as well as in between the  $20\text{ }^{\circ}\text{C}$  and  $30\text{ }^{\circ}\text{C}$  steps. After temperature stabilization a two-hour waiting period before collecting impedance spectroscopy was held to ensure that the whole cell has equilibrated to the desired temperature. In this work we have applied transmission line modelling on the potentiostatic impedance spectra of the electron blocking cells to determine the effective ionic conductivity within the prepared composites. Cells for validation by direct current measurements were prepared by adding 80 mg of  $\text{Li}_6\text{PS}_5\text{Cl}$ , 10 mg of the composite (50 vol.-%  $\text{Li}_6\text{PS}_5\text{Cl}$  and 50 vol.-% Si/C) and another 80 mg of  $\text{Li}_6\text{PS}_5\text{Cl}$  followed by hand-pressing after each step. After the assembly all cells were pressed in a uniaxial press at a pressure of 374 MPa for 3 min. Onto those cells (only for direct current measurements) an indium (chemPUR, 100  $\mu\text{m}$  thickness, 99.99%) disc (9 mm, 50 mg) followed by a freshly pressed lithium (abcr, 99.8%) disc (4 mm, 1.5 mg) were added onto both sides of the cell. Each such cell assembly was put into an aluminum frame and pressure applied by a screw with a torque of 10 Nm (50 MPa) during electrochemical measurements. [18] Polarization measurements using direct current were conducted to determine the effective ionic conductivities using a Metrohm AutoLab Potentiostat (PGSTAT302N). Before the measurement was started an equilibration time of six hours was set. This time was also used to equilibrate the temperature, as new cells were built for each temperature. The applied voltages 2.5 mV; 5 mV; 7.5 mV; 10 mV; 15 mV; 20 mV; and 25 mV were each maintained for three hours to allow the current to stabilize. A one-hour resting period was set between different voltage steps to ensure cell equilibrium. This measurement was performed at five different temperatures ( $5\text{ }^{\circ}\text{C}$ ;  $15\text{ }^{\circ}\text{C}$ ;  $25\text{ }^{\circ}\text{C}$ ;  $40\text{ }^{\circ}\text{C}$ ; and  $60\text{ }^{\circ}\text{C}$ ).

## Results and Discussion

### Transport determination and model validation

Impedance spectroscopy allows to quickly investigate temperature-dependent ionic conductivities when suitable equivalent circuit models are available and validated describing the investigated processes. The determination of the ionic conductivities of pristine solid electrolytes is a well-established procedure that involves fitting the acquired impedance spectra while only considering the total ion transport (see Figure S2). [21] In the case of the effective ionic conductivity within the respective composites this is complicated by the additional impedance response from the electronically conductive carbon in the composites. In this case a TLM can be employed to fit the impedance spectra of a symmetric cell setup (composite | solid electrolyte | composite) obtaining the ionic resistance of the composite. Due to the capabilities of extracting transport parameters, transmission line modeling of electrode composite impedance spectra is used frequently. For instance in NCM622-SE composites by Minnmann *et al.* [16] and Schlautmann *et al.* [24], LiMn<sub>2</sub>O<sub>4</sub>-SE composites by Hendriks *et al.* [17] as well as silicon-carbon-SE composites by Rana *et al.* [11] Furthermore, Ohno *et al.* [25] and König *et al.* [26] successfully employed transmission line modelling to investigate carbon-SE systems applicable to sulfur solid-state cathodes and the ionic transport in wet-milled NCM-Li<sub>5.3</sub>PS<sub>4.3</sub>ClBr<sub>0.7</sub> composites. A TLM-study on the tortuosity of battery electrodes by Landesfeind *et al.* [27] shows that the TLM can successfully be employed for solid-state composites and that the tortuosity factor in these composites is significantly higher compared to the prediction made by Bruggemann Cronau *et al.* for instance used the TLM for a thickness-dependent impedance study of LiCoO<sub>2</sub> cathodes in a liquid electrolyte system, which are generally well understood with transmission line modelling, showing that tortuosity factors are virtually independent electrode thickness between 44  $\mu\text{m}$  and 251  $\mu\text{m}$ . [28] Additionally, it is standard practice to investigate solid oxide fuel cells using the TLM. A three channel TLM was used to model the different loss contributions in anode functional layers and show that a thin substrate with high porosity is beneficial for performance. [29] Furthermore, it was shown that a three channel TLM for double-layered cermet anodes in solid oxide fuel cells offers enhanced accuracy and versatility in simulating anode performance, outperforming the two channel TLM in this use case, and shows that optimizing the electrolyte matrix materials for higher conductivity can significantly improve performance of the anode layer. [30]

The TLM used in this work is shown in **Figure 1a** (also see Eq. S1 & Figure S3). [21] In a previous work it was shown that effective electronic conductivity of the Si/C:Li<sub>6</sub>PS<sub>5</sub>Cl-

composite remains independent of the solid electrolyte content in the range of 0 vol.-% to 50 vol.-%. Additionally, the effective electronic conductivity ( $\sim 2.5 \text{ S} \cdot \text{cm}^{-1}$ ) is four orders of magnitude higher than the best ion conducting composite at room temperature. [10] Therefore, and due to the similarity of the different employed solid electrolytes  $\text{Li}_6\text{PS}_5\text{Br}$  and  $\text{Li}_{1.5}\text{PS}_{4.5}\text{Cl}_{1.5}$  to  $\text{Li}_6\text{PS}_5\text{Cl}$ , the electronic transport is assumed to remain comparably high within all composites prepared. This assumption allows the electronic pathway in the TLM to be well described by a short circuit (i.e. negligible resistances). The impedance spectra show a high-frequency (3 kHz, apex frequency) process that can only be resolved for low temperatures ( $-40^\circ\text{C}$  to  $0^\circ\text{C}$ ). This process can be attributed to the ion transport within the solid electrolyte separator in accordance with the resistivity and capacitance of the pristine solid electrolytes. In the Supporting Information (Figure S3a) an exemplary fit of the low temperature impedance spectra also including the high frequency process is given with the respective equivalent circuit (Figure S3c), confirming that this process is only to be attributed to the separator. [21] By excluding high-frequency responses originating from the separator, it was possible to account for these contributions with a simple resistor and use the same equivalent circuit to analyze all composite impedances throughout this work. The relevant equations for the TLM can be found in the Supporting Information. [21] The capacitances of the ionic pathway are in the range of  $10^{-6} \text{ F}$ . While these are not in the range of bulk capacitances reported for solid electrolytes [31,32], at this stage one may assume the measurement of an average over different processes, for instance additional constriction resistances in the composite and artifacts originating from contacting, that explains the measured range. [33,34]

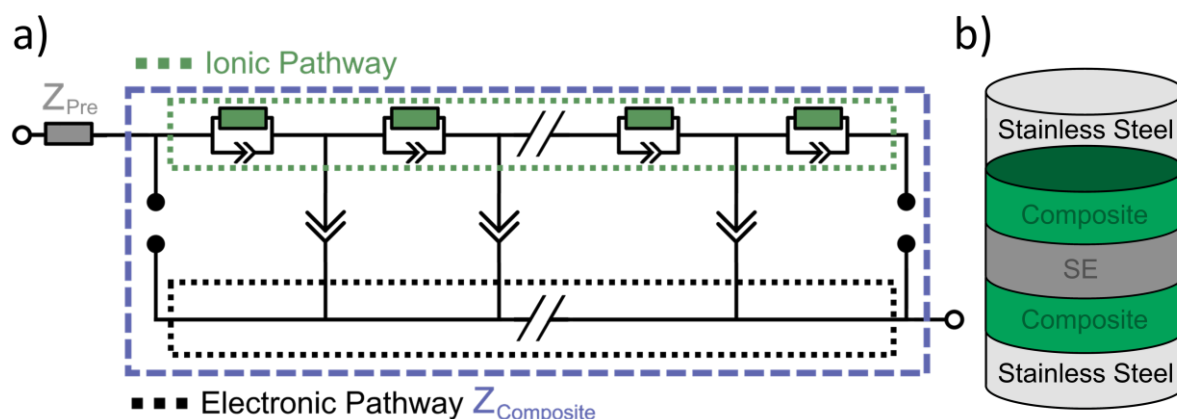


**Figure 1:** a) The employed TLM to determine the effective ionic conductivities of the composites. The impedance response of the composite is modelled by  $Z_{\text{Composite}}$ . While the ionic pathway is highlighted in the dashed green line, the electronic pathway, modelled as a short circuit, is highlighted within the



*dashed black line. The resistance of the  $\text{Li}_6\text{PS}_5\text{Cl}$  separator is given by the resistance  $Z_{\text{Pre}}$ . **b)** Schematic of the cell setup used for the impedance measurements.*

The conductivity data gathered using this TLM was exemplarily verified for the composite containing 50 vol.-%  $\text{Li}_6\text{PS}_5\text{Cl}$ . This was done by building symmetric cells for direct current polarization measurements determining the effective ionic transport at five different temperatures, similar to a previous report. [10] This comparison as well as the schematic cell setup utilized can be found in the Supporting Information (Figure S3b). [21] The comparability of the conductivities from direct current polarization to those obtained from transmission line modelling impedance spectroscopy confirm the validity of the used TLM.

### **Temperature behavior of effective ion transport**

**Figure 2** shows two exemplary impedance spectra of the composites containing 50 vol.-%  $\text{Li}_6\text{PS}_5\text{Cl}$ ,  $\text{Li}_{5.5}\text{PS}_{4.5}\text{Cl}_{1.5}$ , and  $\text{Li}_6\text{PS}_5\text{Br}$  at  $-40\text{ }^\circ\text{C}$  (**Figure 2a**) and  $25\text{ }^\circ\text{C}$  (**Figure 2b**) and the respective fit curves from the TLM. Besides availability and general interest for application in solid-state batteries, these specific solid electrolytes were chosen since  $\text{Li}_6\text{PS}_5\text{Cl}$  and  $\text{Li}_{5.5}\text{PS}_{4.5}\text{Cl}_{1.5}$  show similar activation energies while  $\text{Li}_{5.5}\text{PS}_{4.5}\text{Cl}_{1.5}$  has a significantly higher ionic conductivity. [3,35]  $\text{Li}_6\text{PS}_5\text{Br}$  was chosen as a material with a lower activation energy compared to the Cl-based electrolytes, while still being in the same argyrodite electrolyte family and conductivity range as  $\text{Li}_6\text{PS}_5\text{Cl}$ . [3] When only 30 vol.-% solid electrolyte are contained in the composites, fitting became unreliable at low temperatures ( $-30\text{ }^\circ\text{C}$  and  $-40\text{ }^\circ\text{C}$ ) for Cl-rich argyrodite composites, and at  $60\text{ }^\circ\text{C}$  for the  $\text{Li}_6\text{PS}_5\text{Cl}$  composite, indicated by large uncertainties associated with fitted parameters. However, trends within intermediate temperatures can still be assessed despite these limitations of the modelling at the extreme temperatures at lower volume percentage.

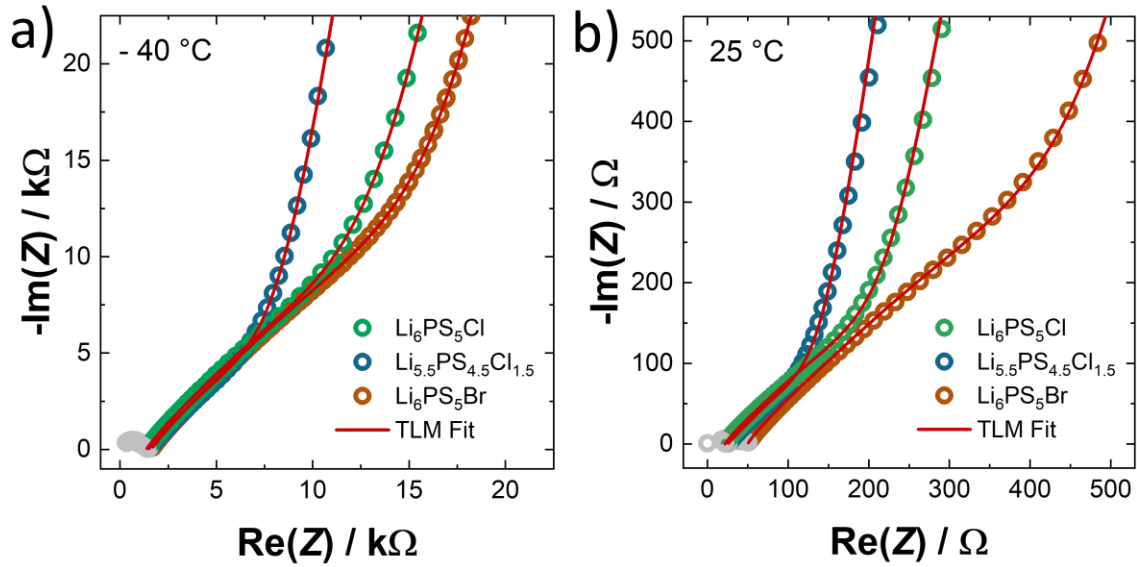


**Figure 2:** Exemplary impedance spectra of the 50 vol.-% composites at  $-40\text{ }^\circ\text{C}$  **a)** and  $25\text{ }^\circ\text{C}$  **b)** with the respective transmission line modelling in red. Data points of the frequency range excluded from fitting are shown in grey.

For all investigated composites, the effective ionic room-temperature conductivity ( $\sigma_{\text{eff, ion, RT}}$ ) scales with the amount of solid electrolyte in the composite (**Figure 3a**). In addition, similarly pronounced changes in the effective ionic conductivity are observed as a function of temperature (Figure S4). [21] All composites show the temperature modified Arrhenius behavior in the change of the effective ionic conductivity with varying temperature as also typically observed in the pure solid electrolytes. An exemplary Arrhenius-type plot of the temperature-dependent effective conductivities in composites containing  $\text{Li}_6\text{PS}_5\text{Cl}$  showcasing the expected linearity is given in **Figure 3b**. All Nyquist plots and respective fits for temperature-dependent conductivities (Figures S6 - S14) as well as Arrhenius plots (Figure S5) are shown in the Supporting Information. [21] As all composites show Arrhenius behavior of the effective ionic conductivity in the investigated temperature range, the activation energies can be calculated from the slope of a linear fit to the respective data (**Figure 3b**). The observed activation energies are given for the pristine solid electrolytes as well as the composites in **Figure 3c**. By reducing the solid electrolyte volume fraction to 40 vol.-% and 30 vol.-% respectively the activation energy increases. This increase is observed for all three evaluated solid electrolytes in their composites from triplicate measurements (**Figure 3c**). The uncertainty of the ionic conductivities is calculated as the standard deviation of the triplicate measurements from one composite per composition measured in three separate cells, the error of the slope on the resulting Arrhenius plot is used to calculate the uncertainty of the activation energies through error propagation.

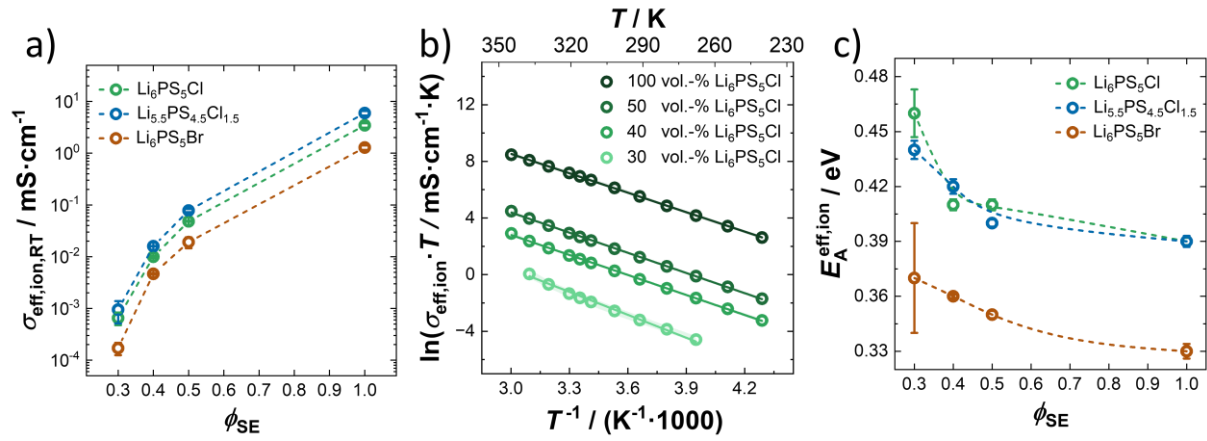


**Figure 3:** **a)** The effective ionic conductivity at room temperature of all investigated composites as well as the respective pristine electrolytes vs. the volume fraction of solid electrolyte, the dashed lines act as guides to the eye. **b)** An exemplary Arrhenius plot for the determination of the activation energies of the  $\text{Li}_6\text{PS}_5\text{Cl}$  composites and the pristine electrolyte. **c)** The activation energies for all composites and electrolytes vs. the volume fraction of solid electrolyte, the dashed lines act as a guide to the eye.

A reasonable question to be asked now is whether the relative increase in activation energy of all composites is the same irrespective of the solid electrolyte used. Normalizing the activation energy of each composite ( $E_{\text{A}}^{\text{ion,eff}}$ ), as well as the one of the pristine electrolytes by the activation energy of the respective pristine electrolyte ( $E_{\text{A}}^{\text{SE}}$ ) yields the relative activation energies ( $E_{\text{A}}^{\text{ion,eff}}/E_{\text{A}}^{\text{SE}}$ ) and allows for a direct comparison. **Figure 4** shows these normalized activation energies and highlights that the changes in  $E_{\text{A}}$  are similar and follow a trend towards higher effective  $E_{\text{A}}$  for lower solid electrolyte volume fractions, within the investigated composites. At 30 vol.-% of the solid electrolyte in the composite, a relative activation energy change of 10% to 20% can be observed. Thus, it is essential to consider the effective ionic transport especially at low temperatures when comparing the loading of cells and the performance evaluation of solid-state composites.

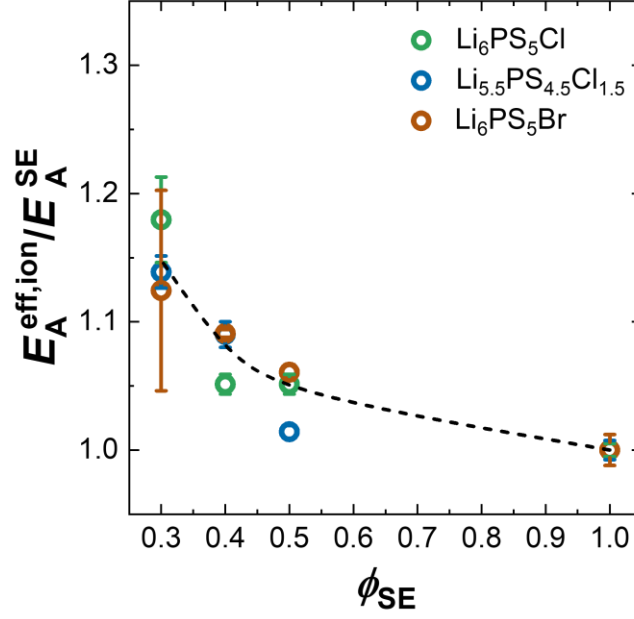


**Figure 4:** The normalized activation energies of the composites of all three electrolytes vs. the volume fraction of solid electrolyte. The dashed line acts as a guide to the eye.

One explanation for the increase in activation energy with decreasing solid electrolyte volume fraction could be a constriction resistance effect on the solid electrolyte – composite interface caused by the reduction in contact area through which lithium transport can happen. [36] Further adding to this hypothesis, temperature-dependent current constriction effects on grain boundaries are possibly contributing to the apparent change in  $E_A$  as the quantity of grain boundary interfaces changes. [37]

### Tortuosity factor consideration and impact on solid-state batteries

From the change in normalized activation energy, the commonly used description of the tortuosity factor  $\kappa$  to assess information about the microstructural pathways in the composites can be investigated on its temperature dependence. [12,15,25,27,38] The most common approach to calculate the tortuosity factor ( $\kappa$ ) is given by:

$$\kappa = \phi_{SE} \frac{\sigma_{SE}}{\sigma_{ion, eff}} \quad (1)$$

The tortuosity factor for solid-state systems is calculated as the product of the volume fraction of the ion conducting phase  $\phi_{SE}$  and the ratio of the ionic conductivity of the pristine solid electrolyte  $\sigma_{SE}$  and the effective ionic transport of the respective composite  $\sigma_{ion, eff}$ . This approach for the determination of the tortuosity factor assumes no temperature dependence. However, as shown in **Figure 3c** the activation energy changes when the volume ratio of solid

electrolyte to active material is changed, resulting in a temperature dependence of  $\kappa$ . This can be shown by assuming Arrhenius behavior for  $\sigma_{SE}$  **Eq. (2)**.

$$\sigma_{SE} = \frac{\sigma_{SE}^0}{T} \exp\left(-\frac{E_A^{SE}}{k_B T}\right) \quad (2)$$

As **Figure 2b** shows linear correlation for the Arrhenius plot ( $\ln(\sigma_{ion,eff} \cdot T)$  vs  $T^{-1}$ ) it can reasonably be assumed that **Eq. (3)** is true for the systems investigated in this work. Combining **Eq. (1)**, **(2)** and **Eq. (3)** and assuming temperature independence for  $\phi_{SE}$  one can define  $\kappa$  as in **Eq. (4)**. The solid electrolyte volume fractions  $\phi_{SE}$  can be assumed to be temperature independent as the volumetric thermal expansion coefficients of all components are sufficiently small being  $-8.7 \cdot 10^{-6} \text{ K}^{-1}$  for graphite [39] and  $7.8 \cdot 10^{-6} \text{ K}^{-1}$  for silicon [40]. The thermal expansion coefficient of  $\text{Li}_{5.5}\text{PS}_{4.5}\text{Cl}_{1.5}$  was assumed to be comparable to that of  $\text{Li}_6\text{PS}_5\text{Cl}$  at  $66 \cdot 10^{-6} \text{ K}^{-1}$  and  $69 \cdot 10^{-6} \text{ K}^{-1}$  for  $\text{Li}_6\text{PS}_5\text{Br}$  which are obtained from Minafra *et al.*, [41] suggesting that there is no difference in volume fraction as a function of temperature for all composites.

$$\sigma_{ion, eff} = \frac{\sigma_{ion, eff}^0}{T} \exp\left(-\frac{E_A^{ion, eff}}{k_B T}\right) \quad (3)$$

$$\kappa = \phi_{SE} \frac{\sigma_{SE}^0}{\sigma_{ion, eff}^0} \exp\left(\frac{E_A^{ion, eff} - E_A^{SE}}{k_B T}\right) \quad (4)$$

This means that if  $E_A^{ion, eff} \neq E_A^{SE}$  is true, which is the case as per **Figure 4**, that there needs to be a  $T$  dependence of  $\kappa$ . This temperature dependance can be observed in the data, while there is not a clear trend at elevated temperatures (above  $\sim 20 \text{ }^\circ\text{C}$ ), there is a visible drop of  $\kappa$  for almost all composites confirming that  $E_A^{ion, eff} \neq E_A^{SE}$ . Composites with higher amounts of solid electrolyte generally exhibit a smaller change of  $\kappa$  compared to composites with less solid electrolyte as can be seen in **Figure 5**. This means that the tortuosity factor  $\kappa$  needs to be

temperature dependent and cannot be a purely geometric factor, highlighting that the tortuosity factor and the geometric tortuosity are not directly related.

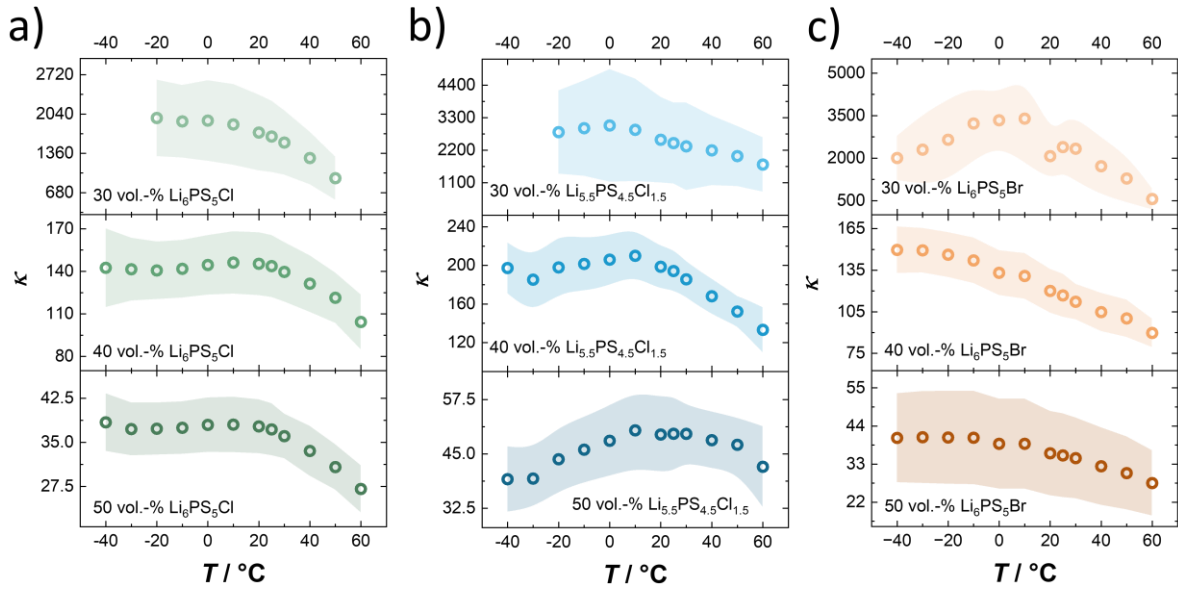


**Figure 5:** Tortuosity factor  $\kappa$  at various temperatures for **a)**  $\text{Li}_6\text{PS}_5\text{Cl}$  in green, **b)**  $\text{Li}_{5.5}\text{PS}_{4.5}\text{Cl}_{1.5}$  in blue and **c)**  $\text{Li}_6\text{PS}_5\text{Br}$  in brown. The  $\kappa$  values and their respective uncertainties through error propagation were calculated using Eq. (1). A temperature dependence is visible. There is no clear trend for low temperatures. However, at temperatures above  $\sim 20$  °C, there is a visible drop of  $\kappa$  for almost all composites.

This work shows that ionic transport in composites is dependent on temperature as well as composition, suggesting that when having more than room-temperature operation as a goal, the transport changes especially at high active material loadings need to be considered. To provide an example of how much changes in ionic transport one would expect by minor changes in the activation energy, **Figure 6:** **a)** shows a theoretical comparison between five different scenarios to show the resulting differences in effective conductivities at high and low temperatures. The activation energy is increased or decreased by 10% and 20%, respectively. As a starting point for the calculation, the room-temperature conductivity of the 50 vol.-%  $\text{Li}_6\text{PS}_5\text{Cl}$  composite  $\sigma = 0.05 \text{ mS}\cdot\text{cm}^{-1}$  as well as the activation energy  $E_A = 0.40 \text{ eV}$  of the pristine electrolyte were chosen. In **Figure 6:** **a)** **a)**, the respective theoretical conductivities are given as a function of temperature and color graded regarding the altering activation energies. It becomes obvious that temperature dependences of the effective ionic conductivities are heavily affected by the changing activation energies. This is emphasized even further by noting the absolute values. In **Figure 6:** **a)** **b)** isotherms interpolated from this case are given, showing the theoretical effective conductivities resulting at the five activation energies. Even at  $T = 0$  °C the impact of a change

in activation energy on the conductivity is already significant, as a 20% increase in activation energy changes the conductivity by nearly 50%. This behavior is accelerated at low temperatures and results in a difference of an order of magnitude at  $T = -40\text{ }^{\circ}\text{C}$  suggesting electrolytes with low activation barriers – or composites with low active material content – are needed for solid-state batteries that run at lower temperatures. While the low activation barriers as a need for fast ionic transport at low temperatures seems trivial, the need for high solid electrolyte content due to the change in activation barriers of the composites is not. In direct contrast to the low-temperature behavior, a higher activation energy may be beneficial for batteries that are operated at elevated temperatures as the conductivity increases faster with increasing temperature when the activation energy is higher. **Figure 6: a) c** shows the three-dimensional dependency of the experimentally determined conductivities of  $\text{Li}_6\text{PS}_5\text{Cl}$  in relation to the composition of the composite and the temperature. The effective ionic transport can be well described by the relatively basic model of the Bruggeman-like effective medium transport combined with the modified Arrhenius behavior found here. It is consequently necessary to take those semi-empirical parameters into account while designing temperature-specific solid-state batteries.

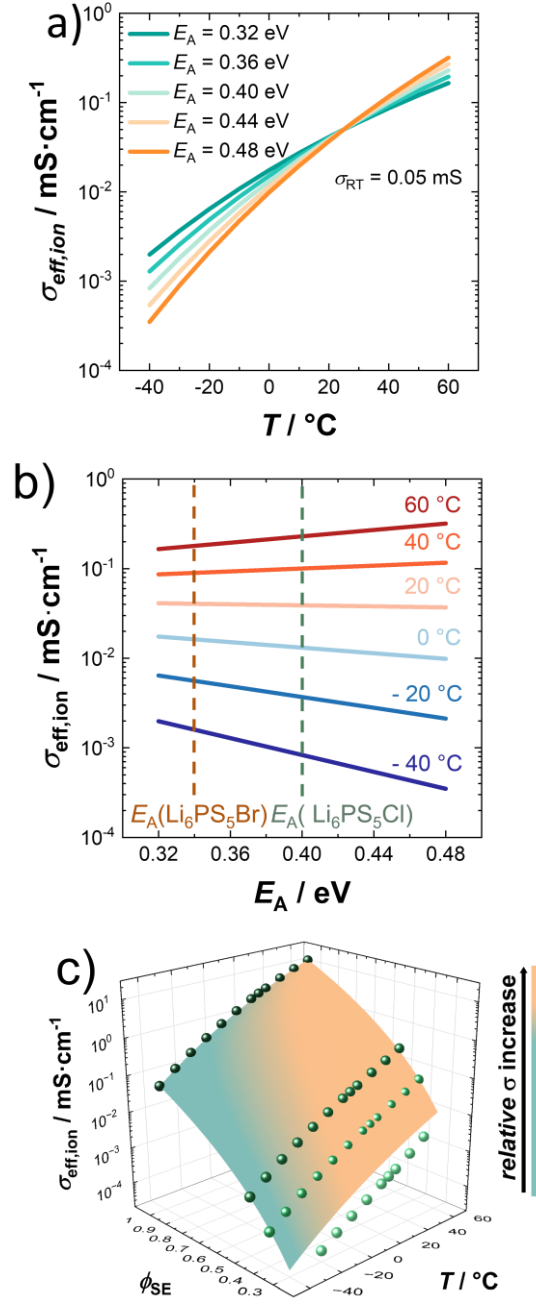


**Figure 6:** **a)** Calculated effective ionic conductivities with changing activation energy of  $E_A(\text{Li}_6\text{PS}_5\text{Cl}) \pm 10\%$  and  $20\%$  at various temperatures. Starting from the activation energy of pristine  $\text{Li}_6\text{PS}_5\text{Cl}$  and the room-temperature conductivity of the 50 vol.-%  $\text{Li}_6\text{PS}_5\text{Cl}$  composite. **b)** Comparison of the isothermal conductivities at the five different activation energies the activation energies of  $\text{Li}_6\text{PS}_5\text{Cl}$  and  $\text{Li}_6\text{PS}_5\text{Br}$  are highlighted in green and brown respectively. **c)** A three-dimensional representation of the  $\text{Li}_6\text{PS}_5\text{Cl}$  conductivity in relation to the composite volume ratio and the temperature. A hypersurface spanning conductivities calculated from the  $\text{Li}_6\text{PS}_5\text{Cl}$  conductivities based on a Bruggeman-type fit. The color of the hypersurface shows the relative change in conductivity with temperature for each composition.



## Conclusion

This work demonstrates how the activation energy of the ion transport is affected by the composition of a solid-state electrode composite utilizing temperature-dependent impedance measurements and transmission line modelling. For three different solid electrolytes ( $\text{Li}_6\text{PS}_5\text{Cl}$ ,  $\text{Li}_{5.5}\text{PS}_{4.5}\text{Cl}_{1.5}$ ,  $\text{Li}_6\text{PS}_5\text{Br}$ ) it was shown that a decrease in the solid electrolyte content in the composite leads to an increase in activation energy. These findings and considerations have a direct impact on the application of solid-state batteries. It has been known for a while that, for a reasonable loading in solid-state batteries a high ionically conducting electrolyte is needed. This work however shows, that besides aiming for a high ionic conductivity at room temperature, the activation energy of the pristine electrolyte also needs to be as low as possible for operation of solid-state batteries at lower temperatures. Otherwise, the decrease in ionic conductivity may be too strongly affecting partial ionic transport in composites. Additionally, by combining the Arrhenius-like description of the temperature dependence with the composition dependence of the ionic conductivity it was shown that the tortuosity factor  $\kappa$  is temperature dependent. Therefore, for fast ionic transport in solid state electrodes composites at low temperatures, low active material loadings are still paramount and more solid electrolyte optimization is clearly needed. Furthermore, it is possible that the influence of electrode composition on the observed activation energy in the sulfide-based electrolytes is transferable to other electrolyte systems, such as oxide and polymer-based systems. However, it is reasonable to assume that the intensity of the observed trend might differ for other electrolyte systems as well as different active materials, as the rigidity and particle sizes of the materials used will likely impact the observed temperature dependence of the effective ionic conductivity. While there has been a tremendous progress on solid-state battery performance at room temperature, the underlying transport characteristics suggest that additional optimization is needed when the operation temperature is changed.

## Supporting Information

In the Supporting Information a Pawley fit of the X-ray diffraction patterns of the solid electrolytes can be found. Furthermore, the volume and mass ratios for all composites are given. The temperature-dependent impedance spectra of all pristine electrolytes with the corresponding equivalent circuits as well as the cell setup are given. The confirmation of the TLM with data gathered from direct current measurements as well as an exemplary fit of low temperature impedance spectra including also the high frequency process for pristine  $\text{Li}_6\text{PS}_5\text{Cl}$

and the 50 vol.-%  $\text{Li}_6\text{PS}_5\text{Cl}$  composite and the equivalent circuit used to fit the 50 vol.-% SE composite are provided as well. Additionally, all temperature-dependent impedance spectra of all composites together with the respective fit and the resulting conductivities are also shown and the Arrhenius plots for  $\text{Li}_{5.5}\text{PS}_{4.5}\text{Cl}_{1.5}$  and  $\text{Li}_6\text{PS}_5\text{Br}$  are given. References cited in the Supporting Information. [17,25]

## Data Availability Statement

The data that support the findings of this study is made available online at <https://doi.org/10.17879/16958461473> through the datastore of the University Münster.

## Acknowledgements

The authors acknowledge financial support within the SilKompAs funded by Bundesministerium für Bildung und Forschung (BMBF project 03XP0486B). Lukas Ketter acknowledge financial support by the International Graduate School for Battery Chemistry. Characterization, Analysis, Recycling, and Application (BACCARA), which is funded by the Ministry for Culture and Science of North Rhine Westphalia, Germany.

## Conflict of Interest

The authors declare no conflict of interest.

## References

- [1] T. Nogueira, E. Sousa, and G. R. Alves, *Electric Vehicles Growth until 2030: Impact on the Distribution Network Power*, Energy Reports **8**, 145 (2022).
- [2] Y. G. Cho, M. Li, J. Holoubek, W. Li, Y. Yin, Y. S. Meng, and Z. Chen, *Enabling the Low-Temperature Cycling of NMC||Graphite Pouch Cells with an Ester-Based Electrolyte*, ACS Energy Lett. **6**, 2016 (2021).
- [3] M. A. Kraft, S. P. Culver, M. Calderon, F. Böcher, T. Krauskopf, A. Senyshyn, C. Dietrich, A. Zevalkink, J. Janek, and W. G. Zeier, *Influence of Lattice Polarizability on the Ionic Conductivity in the Lithium Superionic Argyrodites  $\text{Li}_6\text{PS}_5\text{X}$  ( $\text{X} = \text{Cl}, \text{Br}, \text{I}$ )*, J. Am. Chem. Soc. **139**, 10909 (2017).
- [4] G. W. Kang Yan, Jiangyan Wang, Shuoqing Zhao, Dong Zhou, Bing Sun, Yi Cui, 2019 - *Yan - Temperature-Dependent Nucleation and Growth of Dendrite-Free Lithium Metal Anodes*.Pdf, Angew. Chemie **131**, 11486 (2019).
- [5] J. Janek and W. G. Zeier, *Challenges in Speeding up Solid-State Battery Development*, Nat. Energy **8**, 230 (2023).
- [6] Y. Yang, W. Yuan, W. Kang, Y. Ye, Q. Pan, X. Zhang, Y. Ke, C. Wang, Z. Qiu, and Y. Tang, *A Review on Silicon Nanowire-Based Anodes for next-Generation High-Performance Lithium-Ion Batteries from a Material-Based Perspective*, Sustain. Energy Fuels **4**, 1577 (2020).

- [7] M. T. McDowell, S. W. Lee, W. D. Nix, and Y. Cui, *25th Anniversary Article: Understanding the Lithiation of Silicon and Other Alloying Anodes for Lithium-Ion Batteries*, Adv. Mater. **25**, 4966 (2013).
- [8] P. Vadhva, A. M. Boyce, A. Hales, M.-C. Pang, A. N. Patel, P. R. Shearing, G. Offer, and A. J. E. Rettie, *Towards Optimised Cell Design of Thin Film Silicon-Based Solid-State Batteries via Modelling and Experimental Characterisation*, J. Electrochem. Soc. **169**, 100525 (2022).
- [9] D. Cao, T. Ji, A. Singh, S. Bak, Y. Du, X. Xiao, H. Xu, J. Zhu, and H. Zhu, *Unveiling the Mechanical and Electrochemical Evolution of Nano Silicon Composite Anodes in Sulfide Based All-Solid-State Batteries*, Adv. Energy Mater. **2203969**, 1 (2023).
- [10] Y. Rudel, M. Rana, J. Ruhl, C. Rosenbach, J. Müller, P. Michalowski, A. Kwade, and W. G. Zeier, *Investigating the Influence of the Effective Ionic Transport on the Electrochemical Performance of Si/C-Argyrodite Solid-State Composites*, Batter. Supercaps **6**, 1 (2023).
- [11] M. Rana, Y. Rudel, P. Heuer, E. Schlautmann, C. Rosenbach, M. Y. Ali, H. Wiggers, A. Bielefeld, and W. G. Zeier, *Toward Achieving High Areal Capacity in Silicon-Based Solid-State Battery Anodes: What Influences the Rate-Performance?*, ACS Energy Lett. **8**, 3196 (2023).
- [12] Y. Kato, S. Shiotani, K. Morita, K. Suzuki, M. Hirayama, and R. Kanno, *All-Solid-State Batteries with Thick Electrode Configurations*, J. Phys. Chem. Lett. **9**, 607 (2018).
- [13] L. Peng, C. Yu, Z. Zhang, H. Ren, J. Zhang, Z. He, M. Yu, L. Zhang, S. Cheng, and J. Xie, *Chlorine-Rich Lithium Argyrodite Enabling Solid-State Batteries with Capabilities of High Voltage, High Rate, Low-Temperature and Ultralong Cyclability*, Chem. Eng. J. **430**, 132896 (2022).
- [14] P. Lu et al., *Rate-Limiting Mechanism of All-Solid-State Battery Unravelling by Low-Temperature Test-Analysis Flow*, Energy Storage Mater. **67**, 103316 (2024).
- [15] G. F. Dewald, S. Ohno, J. G. C. Hering, J. Janek, and W. G. Zeier, *Analysis of Charge Carrier Transport Toward Optimized Cathode Composites for All-Solid-State Li–S Batteries*, Batter. Supercaps **4**, 183 (2021).
- [16] P. Minnmann, L. Quillman, S. Burkhardt, F. H. Richter, and J. Janek, *Editors' Choice—Quantifying the Impact of Charge Transport Bottlenecks in Composite Cathodes of All-Solid-State Batteries*, J. Electrochem. Soc. **168**, 040537 (2021).
- [17] T. A. Hendriks, M. A. Lange, E. M. Kiens, C. Baeumer, and W. G. Zeier, *Balancing Partial Ionic and Electronic Transport for Optimized Cathode Utilization of High-Voltage LiMn2O4/Li3InCl6 Solid-State Batteries*, Batter. Supercaps **6**, (2023).
- [18] W. Zhang et al., *Interfacial Processes and Influence of Composite Cathode Microstructure Controlling the Performance of All-Solid-State Lithium Batteries*, ACS Appl. Mater. Interfaces **9**, 17835 (2017).
- [19] K. G. Naik, B. S. Vishnugopi, and P. P. Mukherjee, *Kinetics or Transport: Whither Goes the Solid-State Battery Cathode?*, ACS Appl. Mater. Interfaces **14**, 29754 (2022).
- [20] J. Zahnow, T. Bernges, A. Wagner, N. Bohn, J. R. Binder, W. G. Zeier, M. T. Elm, and J. Janek, *Impedance Analysis of NCM Cathode Materials: Electronic and Ionic Partial Conductivities and the Influence of Microstructure*, ACS Appl. Energy Mater. **4**, 1335 (2021).
- [21] See Supplemental Material at [URL will be inserted by publisher] for more indepth information on the TLM and the validation of the TLM with data gathered from direct current measurements. Temperature dependent conductivity and impedance data for all composites is given as wel, together with the X-ray diffraction patterns of the solid electrolytes.
- [22] J. Müller et al., *Si-on-Graphite Fabricated by Fluidized Bed Process for High-Capacity Anodes*

of Li-Ion Batteries, Chem. Eng. J. **407**, 126603 (2021).

- [23] R. Koerver, W. Zhang, L. De Biasi, S. Schweidler, A. O. Kondrakov, S. Kolling, T. Brezesinski, P. Hartmann, W. G. Zeier, and J. Janek, *Chemo-Mechanical Expansion of Lithium Electrode Materials-on the Route to Mechanically Optimized All-Solid-State Batteries*, Energy Environ. Sci. **11**, 2142 (2018).
- [24] E. Schlautmann et al., *Impact of the Solid Electrolyte Particle Size Distribution in Sulfide-Based Solid-State Battery Composites*, Adv. Energy Mater. **13**, 1 (2023).
- [25] S. Ohno, C. Rosenbach, G. F. Dewald, J. Janek, and W. G. Zeier, *Linking Solid Electrolyte Degradation to Charge Carrier Transport in the Thiophosphate-Based Composite Cathode toward Solid-State Lithium-Sulfur Batteries*, Adv. Funct. Mater. **31**, (2021).
- [26] C. König, V. Miß, L. Janin, and B. Roling, *Mitigating the Ion Transport Tortuosity in Composite Cathodes of All-Solid-State Batteries by Wet Milling of the Solid Electrolyte Particles*, ACS Appl. Energy Mater. **6**, 9356 (2023).
- [27] J. Landesfeind, J. Hattendorff, A. Ehrl, W. A. Wall, and H. A. Gasteiger, *Tortuosity Determination of Battery Electrodes and Separators by Impedance Spectroscopy*, J. Electrochem. Soc. **163**, A1373 (2016).
- [28] M. Cronau, A. Paulus, L. P. Pescara, M. Kroll, D. Renz, J. A. Mekontso, A. Marx, and B. Roling, *What Limits the Rate Capability of Ultrathick Composite Electrodes in Lithium-Ion Batteries? A Case Study on the Thickness-Dependent Impedance of LiCoO<sub>2</sub> Cathodes*, Batter. Supercaps **5**, (2022).
- [29] A. Weber and S. Dierickx, *From Microstructure to Performance: A Detailed Multi-Level Study of SOFC Anodes*, ECS Trans. **91**, 1827 (2019).
- [30] S. Dierickx, T. Mundloch, A. Weber, and E. Ivers-Tiffée, *Advanced Impedance Model for Double-Layered Solid Oxide Fuel Cell Cermet Anodes*, J. Power Sources **415**, 69 (2019).
- [31] I. M. Hodge, M. D. Ingram, and A. R. West, *Impedance and Modulus Spectroscopy of Polycrystalline Solid Electrolytes*, J. Electroanal. Chem. **74**, 125 (1976).
- [32] J. T. S. Irvine, D. C. Sinclair, and A. R. West, *Electroceramics: Characterization by Impedance Spectroscopy*, Adv. Mater. **2**, 132 (1990).
- [33] Y. Liu, Y. Bai, W. Jaegermann, R. Hausbrand, and B. X. Xu, *Impedance Modeling of Solid-State Electrolytes: Influence of the Contacted Space Charge Layer*, ACS Appl. Mater. Interfaces **13**, 5895 (2021).
- [34] A. E. Bumberger, A. Nenning, and J. Fleig, *Transmission Line Revisited – the Impedance of Mixed Ionic and Electronic Conductors*, Phys. Chem. Chem. Phys. **26**, 15068 (2024).
- [35] T. Böger, T. Bernges, Y. Li, P. Canepa, and W. G. Zeier, *Thermal Conductivities of Lithium-Ion-Conducting Solid Electrolytes*, ACS Appl. Energy Mater. **6**, 10704 (2023).
- [36] J. K. Eckhardt, P. J. Klar, J. Janek, and C. Heiliger, *Interplay of Dynamic Constriction and Interface Morphology between Reversible Metal Anode and Solid Electrolyte in Solid State Batteries*, ACS Appl. Mater. Interfaces **14**, 35545 (2022).
- [37] J. K. Eckhardt, S. Kremer, T. Fuchs, P. Minnmann, J. Schubert, S. Burkhardt, M. T. Elm, P. J. Klar, C. Heiliger, and J. Janek, *Influence of Microstructure on the Material Properties of LLZO Ceramics Derived by Impedance Spectroscopy and Brick Layer Model Analysis*, ACS Appl. Mater. Interfaces **15**, 47260 (2023).
- [38] I. V. Thorat, D. E. Stephenson, N. A. Zacharias, K. Zaghib, J. N. Harb, and D. R. Wheeler, *Quantifying Tortuosity in Porous Li-Ion Battery Materials*, J. Power Sources **188**, 592 (2009).
- [39] A. R. H. Monis Abdulmanan Abdullah, Thar Mohammed Badri Albarody, *Graphite Thermal*

*Expansion Coefficient Measured by In-Situ X-Ray Diffraction*, Nanotechnology **31**, 285709 (2020).

- [40] W. M. Yim and R. J. Paff, *Thermal Expansion of AlN, Sapphire, and Silicon*, J. Appl. Phys. **45**, 1456 (1974).
- [41] N. Minafra, M. A. Kraft, T. Bernges, C. Li, R. Schlem, B. J. Morgan, and W. G. Zeier, *Local Charge Inhomogeneity and Lithium Distribution in the Superionic Argyrodites Li<sub>6</sub>PS<sub>5</sub>X (X = Cl, Br, I)*, Inorg. Chem. **59**, 11009 (2020).